第 30 卷第 10 期
2014 年 10 月

无 机 化 学 学 报
CHINESE JOURNAL OF INORGANIC CHEMISTRY

Vol.30 No.10
2425-2432

镍(Ⅲ)-二硫烯配合物的晶体结构与磁性

陈 琪 丁刘锣 焦华晶 芦昌盛*

(南京大学化学化工学院配位化学国家重点实验室,南京 210093)

摘要: 分别以 2-[(4-二甲氨基苯基偶氮]-1-甲基-吡啶阳离子、2-[(4-二甲氨基苯基) 偶氮]-1-苄基-吡啶阳离子和镍-双-1,2-二硫烯阴离子合成了离子对配合物 **1** 和 **2**,并且对 2 个配合物进行了晶体结构和磁性质的研究。晶体 **1** 和 **2** 中,阴阳离子呈柱状交替排列堆积。在 2~300 K 温度范围内,配合物 **1** 具有反铁磁性(θ=−0.016 2 K),配合物 **2** 在 110 K 左右具有 spin-gap 现象(Δ/κ_b= 38 915.42 K)。

关键词: 1,2-二硫烯; 离子对配合物; 晶体结构; 磁性
中图分类号: O614.81+3 **文献标识码**: A **文章编号**: 1001-4861(2014)10-2425-08
DOI:10.11862/CJIC.2014.309

Crystal Structures and Magnetic Behaviors of Nickel(Ⅲ)-Dithiolene Complexes

CHEN Qi DING Liu-Liu JIAO Hua-Jing LU Chang-Sheng*

(*State key Laboratory of Coordination Chemistry, Nanjing University, Nanjing* 210093, *China*)

Abstract: The crystal structures and magnetic properties were investigated for two ion-pair complexes, which consisted of $[Ni(mnt)_2]^-$ (mnt=1,2-dithiolene) with [2-[[4-(dimethylamino)phenyl]azo]-1-methyl-py]$^+$ for complex **1** and [2-[[4-(dimethylamino)phenyl]azo]-1-benzyl-py]$^+$ for complex **2**. In complexes **1** and **2**, cations and anions stacked into segregated columns. Magnetic susceptibility measurements in temperature range 2~300 K showed that complex **1** exhibited an antiferromagnetic coupling feature with θ=−0.016 2 K, while **2** shows characteristic of spin-gap (Δ/κ_b=38915.42 K) around 110 K. CCDC: 993885, **1**; 993887, **2**; 993886, **2′**.

Key words: bis-1,2-dithiolene; ion-pair complex; crystal structure; magnetic property

0 Introduction

The study of molecule-based materials has drawn much attention in the field of solid-state chemistry[1-5]. Inorganic coordination-complex-anions with bis (dithiolene) ligands are proved to be very useful and potential building blocks over the past several decades[6-9]. For example, $[M(mnt)_2]^{n-}$ (M=Ni, Pd, Pt, Cu, Fe; mnt =maleonitriledithiolate) anions have been extensively used as building units in the construction of such molecule-based materials as in the areas of conducting[4,10], magnetic[6-7] and nonlinear optical materials[11]. Interestingly, the ion-pair complexes containing $Ni[(mnt)_2]^-$ anions and certain organic cations can exhibit versatile magnetic properties such as ferromagnetism[12-14], magnetic transition from ferromagnetic to diamagnetic coupling[14], spin-Peierls-like transitions[15-16], and meta-magnetism[17]. It seems that changes of the magnitude and substitutions of the counter-cations shift the overlapping modes of the neighboring $Ni[(mnt)_2]^-$ anions and so that change the magnetic coupling in between[13-19].

收稿日期:2014-03-05。收修改稿日期:2014-04-01。
江苏省自然科学基金(No.BK2011550)资助项目。
*通讯联系人。E-mail:luchsh@nju.edu.cn

In this paper, we synthesized two ion-pair complexes, which consisted of $Ni[(mnt)_2]^-$ as anion, [2-[4-(dimethylamino)-phenyl]azo]-1-methyl-py]$^+$ (**1**) and [2-[[4-(dimethylamino)phenyl]azo]-1-benzyl-py]$^+$ (**2**) as the counter-cations respectively. The cations are able to exhibit *cis-trans* isomerization[20] upon photo-excitation of certain wavelength. Therefore, it is interesting to figure out whether the *cis-trans* isomerization of cations are able to change the crystal structure when photo-excitated under certain wavelength.

1 Experimental

1.1 Chemicals and materials

All reagents and chemicals were purchased from commercial sources and used without further purification. The starting materials $Ni(mnt)_2$[21], [2-[[4-(dimethylamino)phenyl]azo]-1-methyl-py]I[22] and [2-[[4-(dimethylamino)phenyl]azo]-1-benzyl-py]I[23] were prepared in accordance with reported procedures. [2-[[4-(dimethylamino)phenyl]azo]-1-meth-yl-py] $[Ni(mnt)_2]$ and [2-[[4-(dimethylamino)phenyl]azo]-1-benzyl-py][Ni$(mnt)_2$] were obtained by stirring the mixture in MeCN solution of equivalent mole $Ni(mnt)_2$ and [2-[[4-(dimethylamino)phenyl]azo]-1-methyl-py]I or 2-[[4-(dimethylamino)phenyl]azo]-1-benzyl-py]I respectively for 20 min and evaporating under reduced pressure.

1.2 Syntheses of complexes 1 and 2

[2-[[4-(dimethylamino)phenyl]azo]-1-methyl-py][Ni$(mnt)_2$]· MeCN (**1**)

I_2 (150 mg, 0.59 mmol) was slowly added to a MeCN solution (20 mL) of [2-[[4-(dimethylamino) phenyl]azo]-1-methyl-py]$_2$[Ni$(mnt)_2$] (821 mg, 1.0 mmol), and the mixture was stirred for 20 min. Afterwards, diethyl ether (40 mL) was added. The solution was allowed to stand overnight at 4 ℃. Microcrystals (complex **1**, 650 mg) that formed later were filtered off, washed with diethyl ether, and dried in vacuum (~80% yield). Analytical calculation for $C_{22}H_{17}N_8S_4Ni\cdot C_2H_3N$(%): C, 46.39; H, 3.24; N, 20.29. Found for complex **1** (%): C, 46.30; H, 3.18; N, 20.40. Peaks in IR spectrum (KBr disk, cm^{-1}): 3 090 (w), 2 206(vs), 1 606(vs), 1 490(m), 1 302(vs), 1 325(s), 1 161(s), 1 133(vs), 776(s).

[2-[[4-(dimethylamino)phenyl]azo]-1-benzyl-py][Ni$(mnt)_2$] (**2**)

Complex **2** was prepared under the same procedure as in that of complex **1**. Microcrystals (complex **2**, 660 mg) were dried in vacuum (~80% yield). Analytical calculation for $C_{28}H_{20}N_8S_4Ni$(%): C, 38.62; H, 2.29; N, 12.87. Found for complex **2**(%): C, 38.58; H, 2.20; N, 12.81. Peaks in IR spectrum (KBr disk, cm^{-1}): 3 092 (w), 2 206(vs), 1 604(vs), 1 466(w), 1 319(s), 1 252(s), 1 152(s), 1 094(vs), 831(w).

Single crystals of **1** and **2** suitable for X-ray structure analysis were obtained by slowly evaporating solutions of the corresponding complex in MeCN at room temperature for about 7 days.

1.3 Physical measurements

Crystal structure determination was carried out with a Bruker SMART APEX Ⅱ CCD area diffraction and Gemini-Xcalibur X-ray diffractometer. Elemental analysis was performed on a Perkin-Elmer 240 analyzer. Infrared (IR) spectra were recorded on a Bruker Vector 22 instrument as KBr pellets. TG analysis was conducted on a Pyris 1 DSC thermal analyzer (PerkinElmer Company, USA). Powder X-ray diffraction (PXRD) data were collected on a Bruker D8 Advance powder diffraction operating at 40 kV and 40 mA for Cu $K\alpha$ radiation with λ=0.154 18 nm. Magnetic susceptibility data for polycrystalline samples were carried out with a Quantum Design MPMS-5S superconducting quantum interference device (SQUID) magnetometer between 2 ~300 K under a magnetic field of 1 T.

1.4 X-ray single crystallography

Two single crystals with dimensional of 0.18 mm×0.12 mm×0.09 mm and 0.85 mm×0.4 mm×0.2 mm for Crystal **1** and **2** respectively were mounted with an Bruker-SMARTCCD area detector, which was equipped with a graphite monochromatic Mo $K\alpha$ radiation (λ=0.071 073 nm) by using an ψ-ω scan mode at 296(2) K. For crystal **1**, of the total 19 709 reflections collected in the range of 1.36°~28.41°, 7 096 were independent with R_{int}=0.049 0, 3 730 were considered to be observed ($I>2\sigma(I)$) and used in the succeeding refinement; For crystal **2**, of the total of 10 856

reflections collected in the range of 1.32°~28.40°, 7 363 were independent with R_{int}=0.076 0, 5 700 were considered to be observed ($I>2\sigma(I)$) and used in the succeeding refinement. For crystal **2** of 180 K (**2′**) with dimensional of 0.28 mm×0.22 mm×0.17 mm was mounted on a Gemini-Xcalibur X-ray diffractometer with a graphite-monochromatic Mo $K\alpha$ radiation (λ= 0.071 073 nm) by using an ψ-ω scan mode at 180(2) K. A total of 18 557 reflections were collected at the range of 2.85°~25.99° and 5 725 were independent with R_{int}=0.030 9, of which 4 885 were observed with $I>2\sigma(I)$. All the corrections for Lp factors were applied. All structures were solved by direct methods with SHELXS-97 program[24]. The non-hydrogen atoms were anisotropically refined using the full-matrix least-squares method on F^2. All hydrogen atoms were placed at the calculated positions and refined riding on the parent atoms. For crystal **1**, the final refinement including hydrogen atoms converged to R_1=0.046 2, wR_2=0.087 5; R_1=0.045 0, wR_2=0.117 4 for crystal **2** at 296 K and R_1=0.029 8, wR_2=0.078 1 for crystal **2′** at 180 K. Crystallographic data are shown in Table 1.

CCDC: 993885, **1**; 993887, **2**; 993886, **2′**.

2 Results and discussion

2.1 Description of crystal structures

Complex **1** crystallizes in monoclinic space group *C*2/*c*. As showed in Fig.1, the single asymmetric unit explicitly comprises one $[Ni(mnt)_2]^-$ monoanion, one [2-[[4-(dimethylamino)phenyl]azo]-1-methyl-py]$^+$ cation together with one MeCN solvent molecule. In $[Ni(mnt)_2]^-$ moiety, the Ni(Ⅲ) ion is coordinated with four sulfur atoms from two mnt^{2-} ligands, exhibiting a square planar coordination geometry. The average distance of

Table 1　Crystallographic data for compound 1 at 296 K and 2 at 296 K or 180 K

Complex	**1**	**2**	**2′**
Chemical formula	$C_{24}H_{20}N_{10}NiS_4$	$C_{28}H_{21}N_8NiS_4$	$C_{28}H_{21}N_8NiS_4$
Formula weight	621.44	656.5	656.5
Temperature / K	296(2)	296(2)	180(2)
Wavelength / nm	0.071 073	0.071 073	0.071 073
Crystal system	Monoclinic	Triclinic	Triclinic
Space group	*C*2/*c*	$P\bar{1}$	$P\bar{1}$
a / nm	2.563 4(3)	0.766 71(7)	0.754 27(3)
b / nm	0.735 56(10)	1.288 08(12)	1.281 39(5)
c / nm	3.039 6(4)	1.567 19(14)	1.563 55(6)
α / (°)	90	79.211 0(10)	79.321(3)
β / (°)	98.683(2)	88.996 0(10)	89.664(3)
γ / (°)	90	78.625(2)	78.799(3)
V / nm^3	5.665 5(13)	1.490 2(2)	1.456 02(9)
Z	8	2	2
D_c / (g·cm^{-3})	1.457	1.463	1.497
F(000)	2 552	674	674
Limiting indices	$-24 \leqslant h \leqslant 34$, $-9 \leqslant k \leqslant 9$, $-40 \leqslant l \leqslant 40$	$-10 \leqslant h \leqslant 10$, $-17 \leqslant k \leqslant 13$, $-20 \leqslant l \leqslant 20$	$-9 \leqslant h \leqslant 9$, $-15 \leqslant k \leqslant 15$, $-19 \leqslant l \leqslant 19$
Reflections collected / unique	19 709 / 7 096	10 856 / 7 363	18 557 / 5 725
R_{int}	0.049 0	0.076 0	0.030 9
Goodness-of-fit on F^2	1.001	1.004	1.000
Final $R^{a,b}$ indices [$I>2\sigma(I)$]	R_1=0.046 2, wR_2=0.087 5	R_1=0.045 0, wR_2=0.117 4	R_1=0.029 8, wR_2=0.078 1
$R^{a,b}$ indices (all data)	R_1=0.109 4, wR_2=0.106 1	R_1=0.055 4, wR_2=0.124 3	R_1=0.037 1, wR_2=0.082 8

$^aR_1=\sum(||F_o|-|F_c||)/\sum|F_o|$; $^bwR_2=[\sum(|F_o|^2-|F_c|^2)^2/\sum w(|F_o|^2)^2]^{1/2}$.

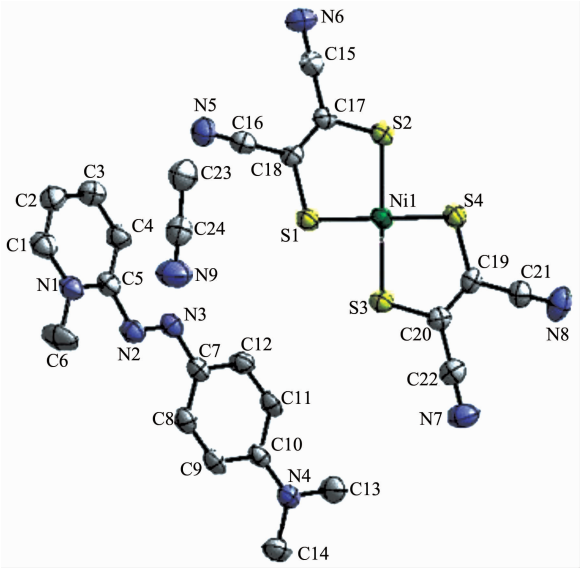

Fig.1 ORTEP view of **1** with non-hydrogen atomic numbering and 30% thermal ellipsoids probability level

Ni-S bonds is 0.214 3 nm, and the average S-Ni-S dihedral angle is 90.000° (Table 2), which are comparable to those of reported data[25].

The anions and cations in complex **1** form regular stacks along the direction of crystallographic *b*-axis. As illustrated in Fig.2(a), the anionic stacks are separated from each other by the cationic packing columns. Two adjacent cations stack in a head-to-tail style to seemingly form a cationic dimer and the phenyl rings are parallel to each other. There are two kinds of weak interactions observed in the cations′ column: (1) $\pi\cdots\pi$ interaction between the benzene rings; (2) C–H···N hydrogen bonds between the C13 atom from the cations and N9 atom from the MeCN molecules, and the C13···N9 distance is 0.347 9 nm. Within the anion stack, two types of alignments are observed with alternating Ni···Ni distances (d_1 and d_2) along the *b*-axis. As shown in Fig.3, in completely overlapping model, the two parallel $[Ni(mnt)_2]^-$ moieties produce such distances as $d_{Ni1\text{-}Ni1\#1}$=0.355 2 nm, $d_{S1\text{-}S3\#1}$=0.355 9 nm, and $d_{S2\text{-}S4\#1}$=0.351 7 nm. However

Table 2 Selected Bond lengths (nm) and angles (°) for 1 and 2

		1			
C(6)-N(1)	0.147 1(4)	C(19)-S(4)	0.170 8(3)	Ni(1)-S(1)	0.214 3(9)
C(17)-S(2)	0.171 1(3)	C(20)-S(3)	0.170 5(3)	Ni(1)-S(3)	0.214 4(9)
C(18)-S(1)	0.170 6(3)	Ni(1)-S(4)	0.213 9(9)	Ni(1)-S(2)	0.214 5(9)
C(2)-C(1)-N(1)	121.50(4)	S(4)-Ni(1)-S(1)	179.06(4)	S(4)-Ni(1)-S(2)	87.33(4)
N(1)-C(5)-N(2)	114.4(3)	S(4)-Ni(1)-S(3)	92.50(4)	S(1)-Ni(1)-S(2)	92.53(3)
N(1)-C(5)-C(4)	117.9(3)	S(1)-Ni(1)-S(3)	87.64(3)	S(3)-Ni(1)-S(2)	179.76(4)
		2			
Ni(1)-S(1)	0.214 8(5)	Ni(1)-S(4)	0.215 3(5)	S(2)-C(26)	0.170 6(2)
Ni(1)-S(2)	0.214 3(6)	S(4)-C(24)	0.172 1(2)	S(1)-C(25)	0.171 3(2)
Ni(1)-S(3)	0.214 6(6)	S(3)-C(23)	0.171 8(2)		
S(2)-Ni(1)-S(3)	179.79(2)	S(2)-Ni(1)-S(4)	87.70(2)	C(7)-C(6)-N(1)	113.45(16)
S(2)-Ni(1)-S(1)	92.35(2)	S(3)-Ni(1)-S(4)	92.51(2)	S(3)-Ni(1)-S(1)	87.45(2)
S(1)-Ni(1)-S(4)	176.92(2)				
		2′			
Ni(1)-S(1)	0.214 6(5)	Ni(1)-S(4)	0.215 0(5)	S(2)-C(26)	0.171 6(19)
Ni(1)-S(2)	0.214 2(5)	S(4)-C(24)	0.172 4(2)	S(1)-C(25)	0.171 1(19)
Ni(1)-S(3)	0.214 6(5)	S(3)-C(23)	0.172 7(19)		
S(2)-Ni(1)-S(4)	87.774(19)	S(2)-Ni(1)-S(1)	92.290(19)	N(1)-C(6)-C(7)	113.50(15)
S(2)-Ni(1)-S(3)	179.64(2)	S(4)-Ni(1)-S(1)	176.40(2)	S(4)-Ni(1)-S(3)	92.481(19)
S(3)-Ni(1)-S(1)	87.471(19)				

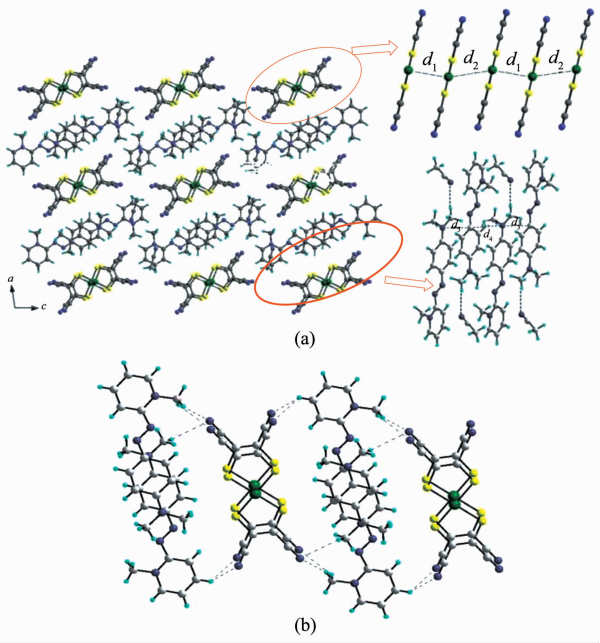

Fig.2　(a) Packing diagram showing the segregated and regular stacks of anions and cations along the crystallographic *b*-axis direction in complex **1**; (b) Hydrogen bonds between anions and cations

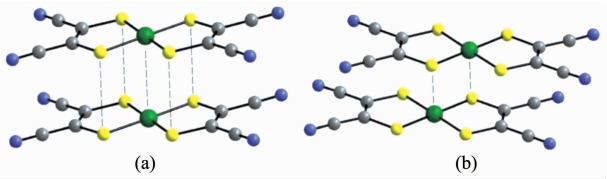

Fig.3　Two types of anion alignments in **1** (completely overlapping with $d_{Ni\text{-}Ni}$=0.355 2 nm (a) and partially overlapping with $d_{Ni\text{-}Ni}$=0.390 0 nm (b))

in partially overlapping model, $[Ni(mnt)_2]^-$ anions slip a little with each other to offer the distances $d_{Ni1\text{-}Ni1\#2}$= 0.390 0 nm, $d_{Ni1\text{-}S1\#2}$=0.373 1 nm. Some weak hydrogen bonds in **1** are list in Table 3. In addition, plane-to-plane distances of the benzene rings between the cations differ slightly, which exhibit d_3=0.366 6 and d_4=0.371 1 nm respectively.

The crystal of **2** at 296 K belongs to triclinic system with space group $P\bar{1}$, and its structure is displayed in Fig.4. As shown in Fig.4, an asymmetric unit consists of one planar $[Ni(mnt)_2]^-$ anion together with one [2-[[4-(dimethylamino)phenyl]azo]-1-benzyl-py]$^+$ cation.

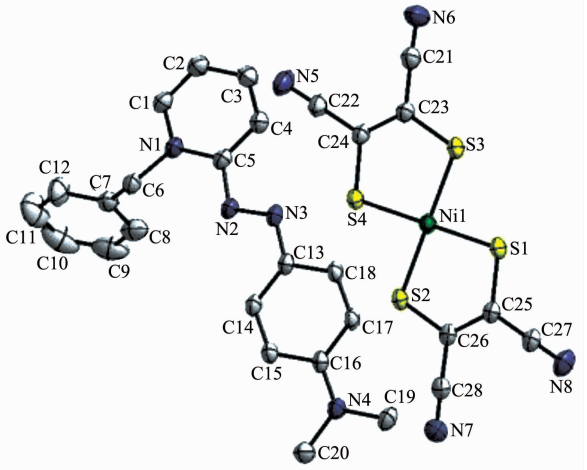

Fig.4　ORTEP view of **2** with non-hydrogen atomic numbering and 30% thermal ellipsoids probability level

The bond lengths of Ni-S are in the range of 0.214 3(5)~0.215 3(6) nm and the angles of S-Ni-S are 87.45(2)° and 92.51(2)° in the $[Ni(mnt)_2]^-$ moiety. For the [2-[[4-(dimethylamino)phenyl]azo]-1-benzyl-py]$^+$ moiety, the azobenzene body is almost planar with a small twist angle of 11.880° between the planes of benzene ring and pyridine ring, with all the bond lengths and angles in normal range. A dihedral between the planes of attached benzyl ring and pyridine ring is 77.399°. The azobenzene body of the cation is almost parallel to the molecular plane of the anion with a dihedral angle of 8.543° (The molecular plane of the anion is defined by four coordinating sulfur atoms).

As displayed in Fig.5, the $[Ni(mnt)_2]^-$ anions and [2-[[4-(dimethylamino)phenyl]azo]-1-benzyl-py]$^+$ cations

Table 3　Hydrogen bonds in complex 1

D–H···A	*d*(D-H) / nm	*d*(H···A) / nm	*d*(D···A) / nm	∠(DHA)/ (°)
C(13)–H(13B)···N(9)#1	0.096	0.254	0.347 9(6)	166.4
C(6)–H(2B)···N(6)#2	0.096	0.254	0.346 8(6)	163.8
C(6)–H(2A)···N(9)#3	0.096	0.262	0.347 7(6)	148.8

Symmetry transformation used to generate equivalent atoms: #1: $-x+1/2$, $-y+3/2$, $-z+2$; #2: $x-1/2$, $y-1/2$, z; #3: $-x+1/2$, $y-1/2$, $-z+3/2$.

form segregated stacks along the anions and [2-[[4-(dimethylamino)phenyl]azo]-1-benzyl-py]$^+$ cations form segregated stacks along the direction of the crystallographic *a*-axis. Both the anion and cation stacks are equidistant owing to the existence of one anion and one cation per cell unit along the direction of the stacks. Thus the neighboring Ni···Ni, N···N distances are equal to the length of the *a*-axis, d_5=0.766 7 nm and d_6=0.766 7 nm within an anion or a cation stack. But the distances within an anion or a cation stack of crystal **2** at 180 K are both 0.754 3 nm, which was 0.012 4 nm shorter than that at 296 K. However, the average bonds length is a little larger at 180 K. This might explain the spin-gap behavior in magnetic susceptibility measurements of complex **2** in the temperature range 2~300 K.

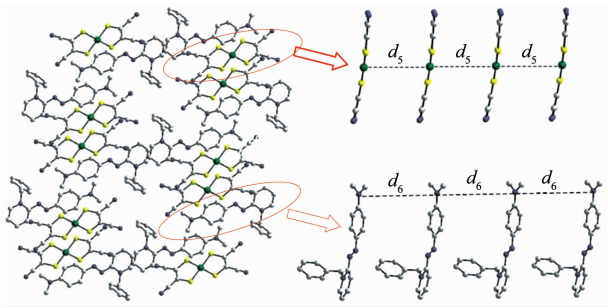

Fig.5 Segregated columnar stack of anions and cations along the direction of *a*-axis in **2** (296 K)

2.2 XRD and Thermogravimetric analysis

The powder X-ray diffraction data for complexes **1** and **2** were collected on a Bruker D8 Avance powder diffraction operating at 40 kV and 40 mA for Cu *Kα* radiation with λ=0.154 2 nm, and were compared with the data simulated with Mercury software. The results were showed in Fig.6. It is experimentally evident that all the peaks in both lines coincide well. So the experimental samples are homogeneous accordingly.

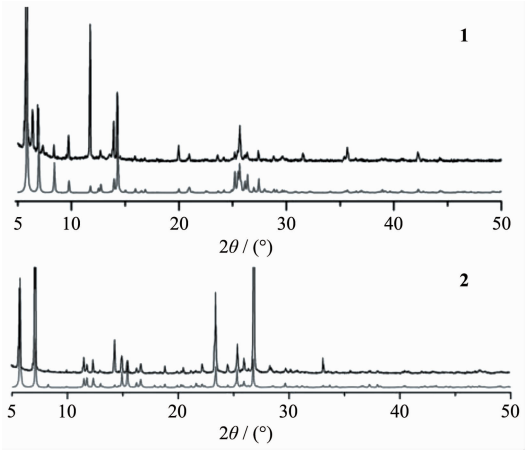

Fig.6 Powder X-ray diffraction pattern of complexes **1** and **2** (upward side lines: experimental; downward side lines: simulated)

Moreover, thermogravimetric analyses were operated as well. As showed in Fig.7, complex **1** is stable up to 80 ℃, and the first weight loss of 6.27% from 80 to 152 ℃ was assigned to the liberation of CH_3CN (Calcd. 6.60%). Above 287 ℃, the framework of complex **1** started to collapse. The framework of complex **2** started to collapse above 260 ℃.

2.3 Magnetic properties

The magnetic properties of complexes **1** and **2** have been determined using polycrystalline samples at temperature range 2~300 K in a field of 2 kOe. The

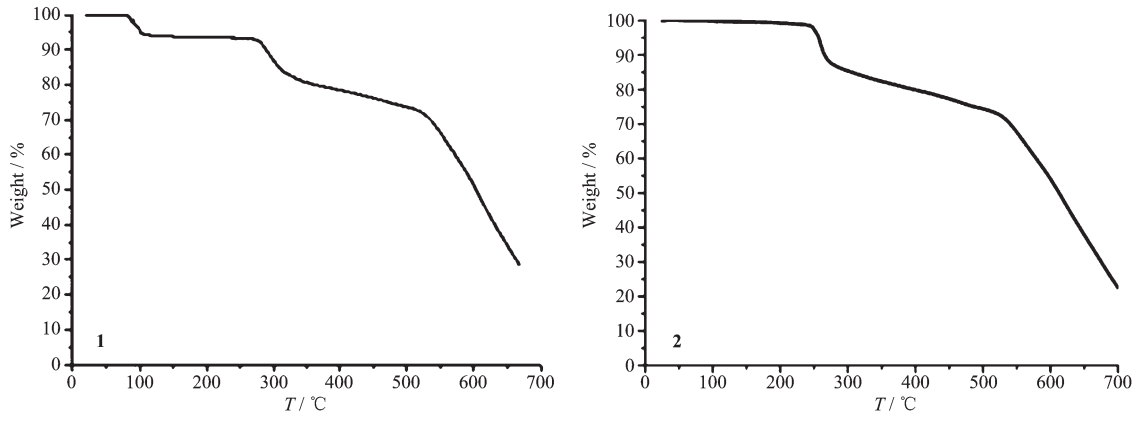

Fig.7 Thermogravimetric analysis of complexes **1** and **2**

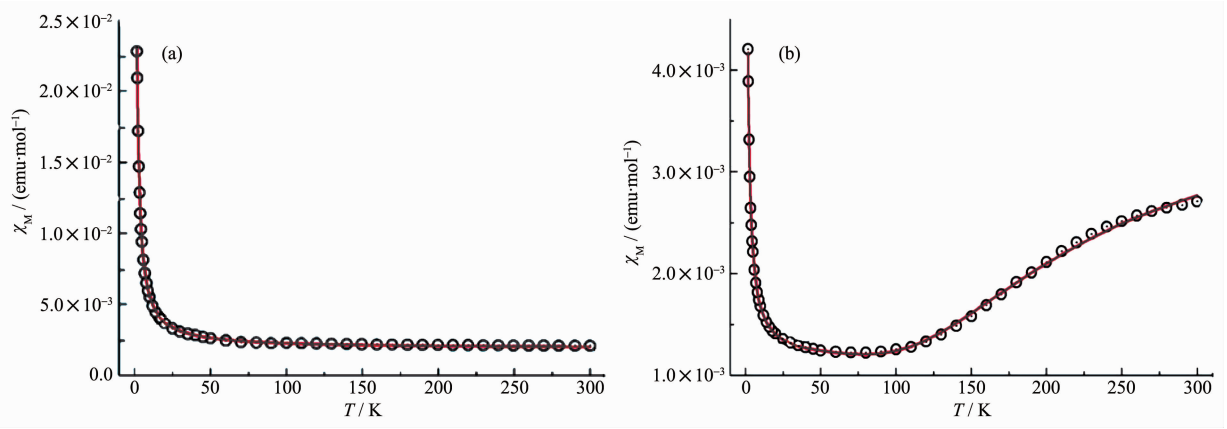

Fig.8　Plots of χ_m vs T of complex **1** (a) and **2** (b), open circles: experimental data, and solid lines: theoretic calculations

results are given in Fig.8. Equation (**1**) was used to fit the temperature dependence of the magnetic susceptibilities of complex **1**:

$$\chi_m=\frac{C}{T-\theta}+\chi_0 \quad (1)$$

The best fitting produced parameters of equation (**1**) with C= 0.037 5 emu·K·mol^{-1}, θ=−0.016 2 K, χ_0= 0.001 8 emu·mol^{-1}. The magnetic susceptibility data within the range of 60~300 K can be finely fitted to the Curie-Weiss law (the circle formed line in Fig.8a).

For complex **2**, when the temperature decreases from 300 K to 110 K, the value of χ_m drops slowly. It is noted that χ_m values decreases exponentially upon cooling at higher temperature region (Fig.8b), indicating that **2** exhibits the characteristics of spin gap[26]. Equation (**2**) was used to fit the temperature dependence of magnetic susceptibilities of complex **2**.

$$\chi_m=\alpha\exp\left(\frac{-\Delta/\kappa_b T}{T}\right)+\frac{C}{T}+\chi_0 \quad (2)$$

Where α is a constant corresponding to the dispersion of excitation energy, Δ is the magnitude of the spin gap, κ_b is the Boltzmann constant, C is a constant corresponding to the contribution of the magnetic impurity, χ_0 contributes from the core diamagnetism and the possible Van Vleck paramagnetism[27]. As observed in Fig.8b (the solid line), equation (**2**) provides a good fit of experimental data. The best fitting yielded the parameters of equation (**2**) with α=0.002 49, Δ/κ_b=38 915.42 K, χ_0= 0.001 13 emu·mol^{-1}, C=0.005 46 emu·K·mol^{-1}.

Reference:

[1] Aziz H, Popovic Z D, Hu N X, et al. *Science*, **1999**,**283**(5409):1900-1902

[2] LI Yue-Hua(李跃华), YANG Zhi-Yi(杨志毅). *J. Dali University*(大理学院学报), **2011**,**10**(4):43-47

[3] DAI Yao-Dong(戴耀东), YU Zhi(余智). *Nature Magazine*(自然杂志), **2002**,**24**(1):15-20

[4] YOU Xiao-Zeng(游效曾). *Molecular-based Materials-Opto Electronic Functional Compounds*(分子材料–光电功能化合物). Shanghai: Shanghai Science and Technology Press, **2001**.

[5] WANG Tian-Wei(王天维), LIN Xiao-Ju(林小驹) WEI Ji-Zong(韦吉宗), et al. *Chinese J. Inorganic Chem.*(无机化学学报), **2002**,**18**(11):1072-1080

[6] Coomber A T, Beljonne D, Friend R H, et al. *Nature*, **1996**, **380**(6570):144-146

[7] Robertson N, Cronin L, *Coord. Chem. Rev.*, **2002**,**227**(1):93-127

[8] Fujita W, Awaga K, Nakazawa Y, et al. *Chem. Phys. Lett.*, **2002**,**352**(5/6):348-352

[9] Canadell E, *Coord. Chem. Rev.*, **1999**,**185**(6):629-651

[10]Tanaka H, Kobayashi H, Kobayashi A, *J. Am. Chem. Soc.*, **2002**,**124**(34):10002-10003

[11]Bigoli F, Chen C T, Wu W C, et al. *Chem. Commun.*, **2001**, **21**:2246-2247

[12]Uruichi M, Yakushi K, Yamashita Y, *J. Mater. Chem.*, **1998**,**8**(1):141-146

[13]Xie J L, Ren X M, Song Y , et al. *J. Chem. Soc., Dalton Trans.*, **2002**(14):2868-2872

[14]Xie J L, Ren X M, Song Y, et al. *Chem. Commun.*, **2002** (20):2346-2347

[15]Ni C L, Dang D B, Song Y, et al. *Chem. Phys. Lett.*, **2004**, **396**(4/5/6):353-358

[16]Ren X M, Meng Q J, Song Y, et al. *Inorg. Chem.*, **2002**,**41**(23):5931-5933

[17]Xie J L, Ren X M, Gao S, et al. *Eur. J. Inorg. Chem.*, **2003**(13):2393-2396

[18]Ni C L, Zhou J R, Tian Z F, et al. *Inorg. Chem. Commun.*, **2007**,**10**(8):880-883

[19]Ni C L, Tian, Z F, Ni, Z P, et al. *Inorg. Chim. Acta*, **2006**, **359**(16):3927-3933

[20]Fritz H L, Swinehart J H, *Inorg. Chem.*, **1975**,**14**(8):935-1939

[21]Davison A, Trop H S, Depamphilis B V, et al. *Inorg. Synth.*, **1982**,**21**:160-162

[22]Prill E A. McElvain S M, *Org. Synth.*, **1935**,**15**:41-44

[23]Mokhtary M, Lakouraj M M. *Chinese Chem. Lett.*, **2011**,**22**(1):13-17

[24]Sheldrick G M, *Acta Crystallogr.*, **1990**,**A46**:467-273

[25]Zuo H R, Huang Q H, Chun Y, et al. *J. Solid State Chem.*, **2009**,**182**(1):147-152

[26]ZHOU Hong(周宏), YU Shan-Shan(于姗姗), DUAN Hai-Bao(段海宝), et al. *Chinese J. Inorg. Chem.*(无机化学学报), **2013**,**29**(7):1375-1384

[27]Isett L C, Rosso D M, Bottger G L, *Phys. Rev. B*, **1980**,**22**(10):4739-4743